Submitted to small

DOI: 10.1002/small.((please add manuscript number))

Grafting Single Molecule Magnets on Gold Nanoparticles

Mauro Perfetti, Francesco Pineider, Lorenzo Poggini, Edwige Otero, Matteo Mannini, Lorenzo Sorace, Claudio Sangregorio, Andrea Cornia, and Roberta Sessoli*

[*] Prof. Roberta Sessoli Corresponding-Author
Department of Chemistry "U. Schiff", Università di Firenze & INSTM RU Firenze,
via della Lastruccia 3, 50019 Sesto Fiorentino (FI), Italy.
roberta.sessoli@unifi.it

Mr. Mauro Perfetti, Dr. Francesco Pineider, Mr. Lorenzo Poggini, Dr. Matteo Mannini, Dr. Lorenzo Sorace, Dr. Claudio Sangregorio
Department of Chemistry "U. Schiff", Università di Firenze & INSTM RU Firenze,
via della Lastruccia 3, 50019 Sesto Fiorentino (FI), Italy.

Dr. Francesco Pineider
Department of Chemistry, Università di Padova, ISTM-CNR & INSTM RU Padova,
via Marzolo, 1 - 35131 Padova, Italy.

Dr. Edwige Otero
Synchrotron Soleil, L'orme des Merisiers Saint-Aubin
BP48 91192 GIF-sur-YVETTE, France

Dr. Claudio Sangregorio
ISTM-CNR via C. Golgi 19, 20133 Milano, Italy

Prof. Andrea Cornia
Department of Chemical and Geological Sciences, Università di Modena e Reggio Emilia & INSTM RU Modena e Reggio Emilia,
via G. Campi 183, 41125 Modena, Italy

Supporting Information is available on the WWW under http://www.small-journal.com or from the author.

Keywords: Single-molecule magnets, nanoparticles, nanomagnetism, synchrotron-radiation, spintronics

Gold nanoparticles are functionalized via ligand exchange using a tetrairon(III) Single-Molecule Magnet (SMM) containing two 1,2-dithiolane end groups. The grafting is evidenced by the shift of the plasmon resonance peak, by NMR spectra, XPS measurements and TEM images. The presence of intact Fe_4 molecules is directly proven by synchrotron-based XAS and XMCD spectroscopy, while a detailed magnetic characterization confirms the persistence of SMM behavior in this new hybrid nanostructure.

1. Introduction

With their giant and directionally-bistable magnetic moment, Single Molecule Magnets (SMMs) are intensely investigated as core components of new molecule-based spintronic devices, in which molecular spins are read-out and manipulated using electric currents.[1],[2] In this direction, a first important step consists in stably interfacing these magnetic molecules with conducting substrates, taking advantage of the perfectly defined and chemically modifiable structure of SMMs.[3] Ultraflat metal substrates,[4] metal nanogaps,[5] graphene nanoconstrictions[6] and carbon nanotubes[7] allowed the electrical addressing of SMMs using STM methods[4] or three-terminal transport measurements.[5-7] The magnetic moment dynamics of SMMs is, however, extremely sensitive to the environment[8] and, since now, only a few types of systems have proven the persistence of slow magnetic relaxation when grafted to metallic surfaces or carbon nanotubes.[9] By inserting a bis(phthalocyaninato)terbium(III) complex in a gold nanojunction, Vincent *et al.* found fingerprints of the tunneling dynamics of the electronic magnetic moment coupled to the nuclear spin.[5a] Moreover, some of us have demostrated that tetrairon(III) (Fe_4) propeller-shaped SMMs with a $S = 5$ ground state retain their magnetic hysteresis once chemically grafted to a gold surface.[9a, 9b] In spite of their low anisotropy barriers ($\Delta \approx 15$ K) and subkelvin blocking temperatures, this class of SMMs exhibits the chemical and structural robustness required even for vapor-phase processing,[10] a very rare property for a polynuclear complex.[11]

We have now explored the chemical grafting of Fe_4 complexes on a third type of metallic substrate, namely gold nanoparticles (Au NPs). Owing to the versatility of the surface chemistry of gold, Au NPs have been functionalized with a wide variety of molecules, ranging from simple capping agents like thiols or amines, to more complex moieties,[12]

including biomolecules and drugs.[13] The rich assortment of functionalities which can be introduced together with the peculiar intrinsic properties of Au NPs has opened exciting perspectives for their application in a wide range of strategic technological areas, such as sensing,[14] nanomedicine,[13-15] and catalysis.[16] Nevertheless, only an isolated and preliminary essay with the very fragile Mn_{12} SMM is documented,[17] and the combination of the optical, transport, and magnetic properties of Au NPs with the quantum magnetization dynamics of SMMs is, to the best of our knowledge, unprecedented. As NPs have enhanced reactivity and are covered by surfactants, the successful extension of the deposition process developed to graft molecules that behave as SMMs on flat surface, on its own rather demanding, is not straightforward. On the other side a hybrid nanostructure constituted by SMMs and NPs would represent a convenient model system to investigate the interaction between SMMs and a conducting substrate. As an important advantage over flat supports, bulk samples of NPs can accommodate much larger quantities of SMMs by virtue of the large surface area of the material. As a consequence, a much wider spectrum of experimental techniques can be applied.

Here we unambiguously show that Au NPs can be successfully functionalized with Fe_4 molecules which retain their SMM behavior in the new hybrid material. The grafting of SMMs promotes extensive aggregation of the NPs, in much the same way as with α-ω-dithiols,[18] suggesting that Fe_4 SMMs can bridge Au NPs through their two sulphur-terminated ligands (see **Figure 1**).

2. Results and discussion

A single batch of several hundreds of milligrams of hexadecylamine (HDA)-capped Au NPs, HDA-NPs hereafter, was prepared modifying a previously reported synthetic procedure (see experimental section) and used for the following exchange reactions after accurate

purification. HDA-NPs were chosen as starting material because the replacement of an N-terminated ligand with a S-terminated one on a gold substrate is a favored process, due to the strong affinity of Au for S. Moreover, HDA was individuated as the best ligand for the exchange reaction due to its compatibility with the SMM, despite other amines are known to provide a better grade of monodispersity.[19] To best exploit the sensitivity of the plasmonic properties to the surface coverage of Au NPs,[20] the experimental conditions were tuned to obtain HDA-NPs with size 5.1±1.2 nm, as shown by the TEM image reported in **Figure 2a** (see SI for methods and statistics). The same batch of HDA-NPs was then used for all ligand exchange experiments. For the functionalization of Au NPs we used a tetrairon(III) complex with a propeller-like structure, $[Fe_4(thioctic)_2(dpm)_6]$ (Fe_4thioctic), where Hdpm is dipivaloylmethane and H_3thioctic is a tripodal proligand obtained by esterification of (±)-α-lipoic acid ("thioctic acid") with pentaerythritol (see Figure 1a). These cyclic disulfides derived from thioctic acid are known to interact strongly with metal surfaces[21] and NPs.[22] The two 1,2-dithiolane rings located on opposite sides of the metal core indeed promote an efficient grafting of Fe_4thioctic on ultraflat gold substrates.[23]

The hybrids were then assembled by exchanging HDA ligands with Fe_4thioctic in CH_2Cl_2 solution (Figure 1b). Based on simple geometrical considerations reported in the SI, an ideal total coverage of the NPs surface requires 12.0 % by weight of Fe_4thioctic. To ensure a complete ligand exchange we added a 2.5 times excess of SMMs. Upon this functionalization, the purple red color, typical of Au NPs of this size, turned to violet-blue and the particles started to flocculate, suggesting the formation of an extended network of Fe_4thioctic-capped NPs (Fe_4-NPs). This allowed the purification of the sample through repeated dispersion in CH_2Cl_2 by sonication and successive spontaneous precipitation over several hours. In contrast, if the sample is treated with ethanol and successively redispersed in a solution of dichloromethane, the red color of the pristine HDA-NPs is restored (see damage proof in SI).

As ethanol is a well-known disrupting agent for Fe_4 core, as shown by XAS-XMCD experiments (see below), this observation supports the hypothesis that aggregation of Fe_4-NPs has to be associated to a double bonding of Fe_4thioctic molecules with NPs. Fe_4-NPs are seen to form extended three-dimensional networks (Figure 2c) where individual NPs can be visualized only at the borders (Figure 2d). Distances between adjacent NPs are shorter than 2.5 nm, thus compatible with the presence of Fe_4thioctic molecules as linker agents.

To prove that the observed behavior is actually induced by the Fe_4thioctic linker, we repeated the same ligand exchange procedure using the methyladamantyl ester of thioctic acid (ADM), which cannot simultaneously bind to two different Au NPs having only one binding site (see SI for the synthetic procedure). No significant color change was detected in this case and no aggregation was observed in TEM images (Figure 2b).

In **Figure 3** we present the normalized plasmon resonance peaks for HDA-NPs, ADM-NPs and Fe_4-NPs in CH_2Cl_2 solution (the complete electronic spectra showing also ligand absorptions are available in SI). HDA-NPs and ADM-NPs display sharp peaks at 522 nm and 530 nm, respectively; this relatively small red-shift is due to the different nature of the ligand donor atoms, as predicted by hard-soft theory.[24] By contrast, Fe_4-NPs manifest a very broadened peak with maximum around 580 nm. It is well-known that aggregation of NPs induces a low-energy shift of the plasmonic peak, which becomes more pronounced on growing the dimension of the aggregate.[25] The observed broad feature for Fe_4-NPs was already observed in literature when a cross-linking agent, like DNA, is added to a solution of gold NPs,[25b] and is therefore indicative of the formation of NPs aggregates, according to TEM image reported in Figure 2c.

The electronic spectra of both Fe_4-NPs and pure Fe_4thioctic feature a common strong absorption peak around 260 nm (see SI), which suggests that the tetrairon(III) core remains intact in the hybrid material.

To exclude that this signal may originate from free Fe_4 complexes in solution, reflecting an instability of the hybrids or their incomplete purification, we used proton Nuclear Magnetic Resonance (^{1}H-NMR). According to several works,[26] when molecules are grafted to NPs the NMR peaks of their protons in closest proximity to the metallic surface undergo a dramatic broadening and may even disappear completely from the spectra. Such an effect is evident if one compares the ^{1}H-NMR spectrum of ADM and of ADM-NPs in CD_2Cl_2: all the signals produced by the 1,2-dithiolane ring protons (δ=1.87-1.95 ppm and δ=2.50-3.62 ppm) become undetectable when the ligand is bound to the metal NP (see SI for further information). The ^{1}H-NMR spectrum of Fe_4thioctic in CD_2Cl_2 is complicated by the paramagnetic nature of the metal ions. It exhibits an intense, broad peak at 10.7 ppm originating from the *t*Bu protons of dipivaloylmethanide ligands,[27] along with very weak and broad signals. A CD_2Cl_2 suspension of Fe_4-NPs features no detectable proton NMR signals, confirming the formation of NPs aggregates that respond as paramagnetic solids (see SI) and indicating that free SMMs are not present in detectable amounts.

To further characterize the Fe_4-NPs hybrid material, we performed X-ray Photoelectron Spectroscopy (XPS) measurements on Au (*4f*), O (*1s*), S (*2p*), Fe (*2p*) and N (*1s*) regions (See SI for experimental spectra and set-up). While Au in the NPs produces an intense peak, the photoemission signals from the other elements are very weak, in agreement with the literature,[28] and almost at the limit of instrumental sensitivity. This is not surprising considering the small percentage of Fe_4thioctic expected in the samples. While not allowing a quantitative analysis, XPS data confirm qualitatively the presence of species containing S and Fe. Notice that an exceedingly weak peak was also detected in the N*1s* region, associated to the contribution of residual HDA ligands.

X-ray absorption spectroscopy (XAS) and X-ray magnetic circular dichroism (XMCD) have been widely employed to investigate surface-supported magnetic molecules. [3, 9a, 9b, 11, 29]

[3, 9a, 9b, 11, 29] [3, 9a, 9b, 11, 29] [3, 9a, 9b, 11, 29] [3, 9a, 9b, 11, 29] [3, 9a, 9b, 11, 29] [3, 9a, 9b, 11, 29] [3, 9a, 9b, 11, 29] [3, 9a, 9b, 11, 29] [3, 9a, 9b, 11, 29] [3, 9a, 9b, 11, 29] [3, 9a, 9b, 11, 29] [3, 9a, 9b, 11, 29] [3, 9a, 9b, 11, 29] [3, 9a, 9b, 11, 29] [3, 9, 11, 29] [3, 9-10, 12, 30] [3, 9, 11, 29] The characterization was performed at the Fe $L_{2,3}$ edges using a low photon flux in order to avoid radiation damage.[30] XAS spectra were measured at a temperature of 2.2 K and under a 30 kOe applied magnetic field parallel to the X-ray propagation vector. The same set-up was used to record the XMCD dependence on the magnetic field to extract an X-ray detected magnetization curve normalized to the isotropic contribution.

XAS spectra are presented in **Figure 4a** for two different circular polarizations of the X-ray beam (σ_- and σ_+). The line shape is typical for Fe_4-based SMMs, which feature iron(III) ions in a distorted octahedral coordination environment. However, additional and conclusive proof of the intactness of the Fe_4 core is provided by the XMCD spectrum. This is defined as the difference in absorption of X-ray with opposite circular polarization ($\sigma^- - \sigma^+$), normalized by the maximum absorption signal in the isotropic spectrum $\frac{1}{2}(\sigma_- + \sigma_+)$. The maximum XMCD amplitude at 709.1 eV (ca. 40%) and the vanishing signal at 707.8 eV are considered fingerprints of the ferrimagnetic spin structure schematized in Figure 1a, where the central and peripheral iron ions provide opposing magnetic contributions.[29] Our synchrotron investigation thus indicates that Au-NPs are capped by intact SMMs. By contrast, when a dichloromethane solution of Fe_4-NPs is treated with ethanol, and the resulting precipitate redissolved in dichloromethane to recover the initial plasmonic peak, a drop-cast sample of this solution shows a much weaker XMCD signal (see SI). The field dependence of the XMCD signal at 709.1 eV was also measured at the same temperature and the results are reported in Figure 4b (see later for further discussion).

With their large surface area, bulk samples of NPs can host a relevant amount of SMMs. Thus, a magnetometric characterization resulted to be feasible.

First, samples of HDA-NPs and ADM-NPs were investigated in order to evaluate the magnetic contribution of the NPs. The magnetization curves at T = 2 K, shown in SI, revealed an increase of the paramagnetic contribution when replacing HDA with 1,2-dithiolane-terminated ADM ligands. This trend has been already observed in other S-functionalized small Au NPs and is attributed to a modification of Au-NPs electronic structure due to the introduction of *5d* band holes upon formation of S-Au bonds.[31] As the paramagnetic signal is expected to change with the coverage of sulphur-terminated ligands, the contribution of Au NPs cannot be directly subtracted from the magnetic data of Fe_4-NPs. However, the magnetization of Fe_4-NPs at 2 K, reported in SI, is ca. one order of magnitude larger than in ADM-NPs, thus allowing a reliable investigation of the magnetic properties of Fe_4 units in the hybrid nanostructure. From the linear part of the *M* vs *H* graph we calculated a susceptibility of $1 \cdot 10^{-4}$ emu g^{-1} at 2 K. At this temperature, the molar χT product of pristine Fe_4thioctic is 13.5 emu K mol^{-1} and the mass percentage of SMM in our sample is therefore estimated as ca. 2.9(3)%. To further confirm the validity of this approach, by comparing the magnetization of Fe_4-NPs and pristine Fe_4thioctic at 2 K and 50 kOe we obtained a rewardingly similar mass percentage of 3.5(3)%.

The SMM behavior of Fe_4 systems is characterized by a well-defined frequency dependent out-of-phase signal in the ac magnetic susceptibility.[10] The in-phase (χ') and out-of-phase (χ'') components of ac susceptibility have been measured on a sample of Fe_4-NPs at variable temperatures in the 100 Hz - 10 kHz frequency range and in both zero and 1 kOe static fields. A field of 1 kOe is in fact able to suppress quantum tunneling of the magnetization without a significant decrease in the susceptibility due to saturation effects. The results, reported in SI, have been analyzed using the Casimir and Du Pré formula[45] to extract the relaxation time (τ) as well as the distribution width of τ through the empirical parameter α. The data in **Figure 5** (circles) show that $\ln\tau$ is a linear function of T^{-1} indicating that magnetic relaxation takes

place *via* thermal activation. A linear fit was then performed to obtain the height of the anisotropy barrier (Δ) and the pre-exponential factor (τ_0) in the Arrhenius law, $\tau = \tau_0 \exp(\Delta/k_B T)$. The values extracted from the fit are: (at H = 0 Oe) Δ = 8.0(1) K and τ_0 = 1.20(6)·10^{-6} s; (at H = 1 kOe) Δ = 11.6(1) K, τ_0 = 1.01(4)·10^{-6} s. Noticeably, the distribution width of relaxation times displayed in Figure 5 (triangles) is about twice broader than in crystalline Fe$_4$thioctic.[23]

In order to obtain information on the magnetic anisotropy responsible for slow magnetic relaxation, we recorded W-band (95 GHz) EPR spectra on solid Fe$_4$-NPs at variable temperature (**Figure 6**). The Fe$_4$-NPs were measured directly as a powder, while control spectra of microcrystalline Fe$_4$thioctic were measured blocking the powder in wax to avoid preferential orientation of the microcrystallites which may occur on application of magnetic field.

The spectra show the fine structure typical of a zero-field split ground state and their temperature dependence confirms the easy axis character of the investigated system.[32] Indeed, the spectra compare very well with those obtained on a microcrystalline sample of Fe$_4$thioctic, suggesting a strict similarity of the anisotropy parameters in the pristine material and in the hybrid nanostructure. For a quantitative estimation of the anisotropy parameters we undertook spectral simulations[33] based on the following spin Hamiltonian:

$$\widehat{H}_{EPR} = D[\hat{S}_z^2 - S(S+1)/3] + E(\hat{S}_x^2 - \hat{S}_y^2) + B_4^0 \widehat{\boldsymbol{O}}_{\boldsymbol{4}}^{\boldsymbol{0}} + g\mu_B \widehat{\mathbf{H}} \cdot \widehat{\boldsymbol{S}}$$

A good agreement between calculated and experimental spectra of Fe$_4$-NPs was obtained with the following parameters: S = 5, D = -0.415(2) cm^{-1}, E = 0.010(1) cm^{-1} and B_4^0 = 1.0(1) × 10^{-5} cm^{-1} while g was fixed at 2.000(5), as expected for high-spin iron(III)-containing species. Inclusion of higher order anisotropy terms is generally necessary to correctly describe the

EPR spectra of SMMs, which are intrinsically multi-spin in nature.[34] The peculiar variation of linewidth along the spectrum has been accounted for by imposing different and anisotropic linewidth parameters for different groups of resonances. The *D* parameter estimated from EPR spectra was employed to simulate the X-ray detected magnetization curve at low temperature. As shown in Figure 4b, the result scales very well with the XMCD data, which are unaffected by the paramagnetic contribution of the Au NPs.

Based on the above described EPR studies, the total splitting of the $S = 5$ manifold is $|D|S^2/k_B = 14.9$ K, to be compared to the effective barrier of about 8 K obtained by AC magnetic measurements. This observation suggests the presence of an efficient tunnel mechanism, also confirmed by the marked increase of the barrier height when the energy degeneracy of the $\pm m_s$ pairs is lifted by application of a static magnetic field. Although such an effect of the static field is quite common among SMMs, crystalline Fe_4 derivatives, including Fe_4thioctic, exhibit a much weaker field effect. The pronounced tunnel efficiency in zero field could in principle be attributed to structural distortions induced by the formation of the NPs aggregates. However, a comparison with the Spin Hamiltonian parameters reported for crystalline Fe_4thioctic, $D = -0.430(4)$ cm^{-1} and $E = 0.005(2)$ cm^{-1},[31] indicates that the zero-field splitting parameters do not change much upon grafting to the Au NPs. Differences in higher-order transverse terms cannot be ruled out at this stage, since these important sources of tunneling[34] have basically no effect on the EPR spectra of randomly-oriented samples. The observed enhancement of quantum tunneling in zero field however suggests that other mechanisms might be active, which are possibly related to the metallic nature of the substrate and require further studies. In this respect, the grafting of SMMs on NPs rather than on ultraflat surfaces seems a very convenient strategy to investigate such substrate-dependent effects, as the dynamics of the magnetization can be directly probed over a wide frequency range via traditional ac susceptometry.

3. Conclusions

In conclusion, we prepared and characterized Fe_4thioctic-capped gold NPs, a new material that combines the magnetic bistability of SMMs with the plasmonic and transport properties of gold NPs. The SMM behavior is preserved, with an increased efficiency of the tunnel mechanism that cannot be simply attributed to a distortion of cluster's geometry, caused by the intense strain inside the NPs aggregates. The metallic nature of the NPs could play a role here and it would be interesting to investigate if the excitation of localized plasmon resonance is able to affect the magnetization dynamics of the SMMs. Although the large aggregates obtained here are not suitable for transport measurements in nano-juctions, where isolated NPs are required, they might be employed in mesoscopic devices. Interestingly, our functionalization procedure can be adapted to grow the network layer-by-layer directly on the electrodes, as commonly done for di-thiol-functionalized NPs employed for gas sensing.[28d] The replacement of Au NPs with magnetic alloys is also an interesting extension of the approach to realize hybrid magnetic materials and investigate quantum effects in magneto-transport devices without requiring the manipulation of isolated SMMs.

4. Experimental Section

Synthesis

Unless otherwise stated, all reagents were purchased from Sigma Aldrich with purity at least 98%.

HDA-capped gold NPs were prepared by slight modification of literature procedures.[19, 35] In a 250 mL three-neck flask, 25 g of HDA were solubilized in 160 mL of $CHCl_3$ at 40°C under N_2 flow and vigorous magnetic stirring. When the solution became colorless, a solution of 0.9 g of $HAuCl_4 \cdot 4H_2O$ (purchased from Strem Chemicals) in 5 mL of $CHCl_3$ was rapidly added. The mixture, heated to reflux, assumed a red color and, after 10 min, turned to orange.

A solution of 0.3 g of tert-butylamineborane complex in 5 mL of $CHCl_3$ was then quickly added. The obtained purple-red mixture was stirred under N_2 atmosphere for 1 h and cooled down to room temperature. Ethanol (340 ml) was added to give a violet solution that was centrifuged at 5,000 rpm for 5 min, discarding the supernatant. The dark-red precipitate was solubilized in a small volume of CH_2Cl_2 (15 ml) and ethanol was added (30 ml) before centrifugation. The washing procedure was repeated four times to obtain a purple-red solution containing ca. 200 mg of HDA-capped gold NPs in 50 ml of CH_2Cl_2. The average diameter of the synthesized NPs was 5.1±1.2 nm, as estimated from TEM images (see SI for statistics).

To obtain ADM-capped gold NPs, a 2.5 times excess of ADM (41 mg) was added to a solution of 60 mg of HDA-capped gold NPs in 15 mL of CH_2Cl_2 and the mixture was stirred for 24 h at room temperature. The adopted purification procedure was similar to that reported for HDA-capped NPs, with ethanol replaced by methanol to decrease the solvent affinity of ADM-NPs. A purple-red solution was finally obtained.

Au NPs capped by Fe_4thioctic were obtained by introducing a 2.5 times excess of Fe_4thioctic[23] (30 mg) in a solution of 100 mg of HDA-capped gold NPs in 25 mL of CH_2Cl_2. The mixture was stirred for 24 h at room temperature. In this case the NPs started to flocculate, so the purification occurred via direct precipitation from the solution over several hours; the initially yellow supernatant was discarded, the black precipitate dispersed again in CH_2Cl_2 and the washing-cycle repeated six times to finally afford a colorless solution over a dark precipitate. Fe_4-NPs have a low solubility in CH_2Cl_2, so prolonged sonication was necessary to get a violet-blue solution.

Characterization

TEM images were obtained using a CM12 PHILIPS TEM, equipped with an OLYMPUS megaview G2 camera, resolution power of 0.34 nm and emitter filament tension of 100 kV.

UV-Vis spectra were recorded with a JASCO V-670 spectrophotometer. XAS and XMCD characterizations were performed at the DEIMOS beamline of Soleil synchrotron facility (France) on a sample of precipitated Fe_4-NPs deposited mechanically on a Cu foil. The UHV compatible pumped ^{4}He optical cryomagnet of the beamline was used and absorption spectra measured in Total-Electron Yield (TEY) detection mode[36] to guarantee an optimal detection sensitivity. The static and dynamic magnetic properties were measured on powders with teflon coverage in a Quantum Design MPMS SQUID and in a Quantum Design PPMS systems equipped with the alternating current measurement option. EPR spectra were recorded using a Bruker E600 continuous-wave spectrometer with a cylindrical cavity (TE011 mode) operating around 94 GHz equipped with a split-coil superconducting magnet (Oxford instruments) and a continuous flow cryostat (Oxford CF935), to achieve temperature variation.

References

[1] L. Bogani, W. Wernsdorfer, *Nat. Mater.* **2008**, *7*, 179-186.

[2] K. V. Raman, A. M. Kamerbeek, A. Mukherjee, N. Atodiresei, T. K. Sen, P. Lazić, V. Caciuc, R. Michel, D. Stalke, S. K. Mandal, *Nature* **2013**, *493*, 509-513.

[3] aN. Domingo, E. Bellido, D. Ruiz-Molina, *Chem. Soc. Rev.* **2012**, *41*, 258-302; bA. Cornia, M. Mannini, P. Sainctavit, R. Sessoli, *Chem. Soc. Rev.* **2011**, *40*, 3076-3091.

[4] aT. Komeda, H. Isshiki, J. Liu, Y.-F. Zhang, N. Lorente, K. Katoh, B. K. Breedlove, M. Yamashita, *Nat Commun* **2011**, *2*, 217; bS. Kahle, Z. Deng, N. Malinowski, C. Tonnoir, A. Forment-Aliaga, N. Thontasen, G. Rinke, D. Le, V. Turkowski, T. S. Rahman, S. Rauschenbach, M. Ternes, K. Kern, *Nano Lett.* **2012**, *12*, 518-521; cJ. Schwöbel, Y. Fu, J. Brede, A. Dilullo, G. Hoffmann, S. Klyatskaya, M. Ruben, R. Wiesendanger, *Nat. Commun.* **2012**, *3*, 953.

[5] aR. Vincent, S. Klyatskaya, M. Ruben, W. Wernsdorfer, F. Balestro, *Nature* **2012**, *488*, 357-360; bE. Burzurí, A. Zyazin, A. Cornia, H. Van der Zant, *Phys. Rev. Lett.* **2012**, *109*, 147203.

[6] A. Candini, S. Klyatskaya, M. Ruben, W. Wernsdorfer, M. Affronte, *Nano Lett.* **2011**, *11*, 2634-2639.

[7] M. Urdampilleta, S. Klyatskaya, J. P. Cleuziou, M. Ruben, W. Wernsdorfer, *Nat. Mater.* **2011**, *10*, 502-506.

[8] aL. Malavolti, M. Mannini, P.-E. Car, G. Campo, F. Pineider, R. Sessoli, *J. Mater. Chem. C* **2013**; bA. Hofmann, Z. Salman, M. Mannini, A. Amato, L. Malavolti, E. Morenzoni, T. Prokscha, R. Sessoli, A. Suter, *ACS Nano* **2012**, *6*, 8390-8396.

[9] aM. Mannini, F. Pineider, P. Sainctavit, C. Danieli, E. Otero, C. Sciancalepore, A. M. Talarico, M. A. Arrio, A. Cornia, D. Gatteschi, R. Sessoli, *Nat. Mater.* **2009**, *8*, 194-

197; bM. Mannini, F. Pineider, C. Danieli, F. Totti, L. Sorace, P. Sainctavit, M. A. Arrio, E. Otero, L. Joly, J. C. Cezar, A. Cornia, R. Sessoli, *Nature* **2010**, *468*, 417-421; cS. Kyatskaya, J. Ramon Galan-Mascaros, L. Bogani, F. Hennrich, M. Kappes, W. Wernsdorfer, M. Ruben, *J. Am. Chem. Soc.* **2009**, *131*, 15143-15151; dA. Giusti, G. Charron, S. Mazerat, J. D. Compain, P. Mialane, A. Dolbecq, E. Riviere, W. Wernsdorfer, R. N. Bibouni, B. Keita, L. Nadjo, A. Filoramo, J. P. Bourgoin, T. Mallah, *Angewandte Chemie-International Edition* **2009**, *48*, 5049-5052; eG. Charron, A. Giusti, S. Mazerat, P. Mialane, A. Gloter, F. Miserque, B. Keita, L. Nadjo, A. Filoramo, E. Riviere, W. Wernsdorfer, V. Huc, J. P. Bourgoin, T. Mallah, *Nanoscale* **2010**, *2*, 139-144; fL. Bogani, C. Danieli, E. Biavardi, N. Bendiab, A. Barra, E. Dalcanale, W. Wernsdorfer, A. Cornia, *Angewandte Chemie-International Edition* **2009**, *48*, 746-750.

[10] L. Margheriti, M. Mannini, L. Sorace, L. Gorini, D. Gatteschi, A. Caneschi, D. Chiappe, R. Moroni, F. Buatier de Mongeot, A. Comia, F. M. Piras, A. Magnani, R. Sessoli, *Small* **2009**, *5*, 1460-1466.

[11] V. Corradini, A. Ghirri, E. Garlatti, R. Biagi, V. De Renzi, U. del Pennino, V. Bellini, S. Carretta, P. Santini, G. Timco, *Adv. Funct. Mater.* **2012**, 3706-3713.

[12] M.-C. Daniel, D. Astruc, *Chem. Rev. Columb.* **2004**, *104*, 293.

[13] L. Dykman, N. Khlebtsov, *Chem. Soc. Rev.* **2012**, *41*, 2256-2282.

[14] aJ. N. Anker, W. P. Hall, O. Lyandres, N. C. Shah, J. Zhao, R. P. Van Duyne, *Nat. Mater.* **2008**, *7*, 442-453; bK. M. Mayer, J. H. Hafner, *Chem. Rev.* **2011**, *111*, 3828.

[15] R. A. Sperling, P. R. Gil, F. Zhang, M. Zanella, W. J. Parak, *Chem. Soc. Rev.* **2008**, *37*, 1896-1908.

[16] M. Stratakis, H. Garcia, *Chem. Rev.* **2012**, *112*, 4469-4506.

[17] G. Balaji, G. Bovenkamp, V. Palshin, C. Kumar, in *MRS Proceedings, Vol. 1198*, Cambridge Univ Press, **2009**.

[18] T. Ogawa, K. Kobayashi, G. Masuda, T. Takase, S. Maeda, *Thin Solid Films* **2001**, *393*, 374-378.

[19] S. Peng, Y. Lee, C. Wang, H. Yin, S. Dai, S. Sun, *Nano Res.* **2008**, *1*, 229-234.

[20] M. M. Alvarez, J. T. Khoury, T. G. Schaaff, M. N. Shafigullin, I. Vezmar, R. L. Whetten, *J. Phys. Chem. B* **1997**, *101*, 3706-3712.

[21] L.-Y. Zhang, H.-X. Zhang, S. Ye, H.-M. Wen, Z.-N. Chen, M. Osawa, K. Uosaki, Y. Sasaki, *Chem. Commun.* **2011**, *47*, 923-925.

[22] aR. Klajn, L. Fang, A. Coskun, M. A. Olson, P. J. Wesson, J. F. Stoddart, B. A. Grzybowski, *J. Am. Chem. Soc.* **2009**, *131*, 4233-4235; bJ. M. Abad, S. F. Mertens, M. Pita, V. M. Fernández, D. J. Schiffrin, *J. Am. Chem. Soc.* **2005**, *127*, 5689-5694; cS. Berchmans, P. J. Thomas, C. Rao, *J. Phys. Chem. B* **2002**, *106*, 4647-4651.

[23] M. J. Rodriguez-Douton, M. Mannini, L. Armelao, A. L. Barra, E. Tancini, R. Sessoli, A. Cornia, *Chem. Commun.* **2011**, *47*, 1467-1469.

[24] S. K. Ghosh, S. Nath, S. Kundu, K. Esumi, T. Pal, *J. Phys. Chem. B* **2004**, *108*, 13963-13971.

[25] aS. Lin, M. Li, E. Dujardin, C. Girard, S. Mann, *Adv. Mater.* **2005**, *17*, 2553-2559; bJ. J. Storhoff, A. A. Lazarides, R. C. Mucic, C. A. Mirkin, R. L. Letsinger, G. C. Schatz, *J. Am. Chem. Soc.* **2000**, *122*, 4640-4650.

[26] aA. Badia, S. Singh, L. Demers, L. Cuccia, G. R. Brown, R. B. Lennox, *Chem. Eur. J.* **2006**, *2*, 359-363; bA. Badia, W. Gao, S. Singh, L. Demers, L. Cuccia, L. Reven, *Lang.* **1996**, *12*, 1262-1269; cR. H. Terrill, T. A. Postlethwaite, C. Chen, C. D. Poon, A. Terzis, A. Chen, J. E. Hutchison, M. R. Clark, G. Wignall, *J. Am. Chem. Soc.* **1995**, *117*, 12537-12548.

[27] E. Tancini, M. J. Rodriguez-Douton, L. Sorace, A. L. Barra, R. Sessoli, A. Cornia, *Chem. Eur. J.* **2010**, *16*, 10482-10493.
[28] aD. G. Castner, K. Hinds, D. W. Grainger, *Lang.* **1996**, *12*, 5083-5086; bS. P. Chenakin, B. Heinz, H. Morgner, *Surf. Sci.* **1999**, *421*, 337-352; cK. Heister, M. Zharnikov, M. Grunze, L. Johansson, *J. Phys. Chem. B* **2001**, *105*, 4058-4061; dY. Joseph, I. Besnard, M. Rosenberger, B. Guse, H. G. Nothofer, J. M. Wessels, U. Wild, A. Knop-Gericke, D. Su, R. Schlögl, *J. Phys. Chem. B* **2003**, *107*, 7406-7413.
[29] M. Mannini, E. Tancini, L. Sorace, P. Sainctavit, M. A. Arrio, Y. Qian, E. Otero, D. Chiappe, L. Margheriti, J. C. Cezar, R. Sessoli, A. Cornia, *Inorg. Chem.* **2011**, *50*, 2911-2917.
[30] M. Mannini, P. Sainctavit, R. Sessoli, C. C. D. Moulin, F. Pineider, M. A. Arrio, A. Cornia, D. Gatteschi, *Chem. Eur. J.* **2008**, *14*, 7530-7535.
[31] P. Crespo, R. Litrán, T. Rojas, M. Multigner, J. De la Fuente, J. Sánchez-López, M. Garcia, A. Hernando, S. Penadés, A. Fernández, *Phys. Rev. Lett.* **2004**, *93*, 87204.
[32] D. Gatteschi, A. L. Barra, A. Caneschi, A. Cornia, R. Sessoli, L. Sorace, *Coord. Chem. Rev.* **2006**, *250*, 1514-1529.
[33] C. J. H. Jacobsen, E. Pedersen, J. Villadsen, H. Weihe, *Inorg. Chem.* **1993**, *32*, 1216-1221.
[34] D. Gatteschi, R. Sessoli, J. Villain, *Molecular nanomagnets*, Oxford University Press, Oxford, UK, **2006**.
[35] X. Hou, X. Zhang, Y. Fang, S. Chen, N. Li, Q. Zhou, *J. Nanopart. Res.* **2011**, *13*, 1929-1936.
[36] R. Nakajima, J. Stohr, Y. U. Idzerda, *Physical Review B* **1999**, *59*, 6421-6429.

Acknowledgements

We thank the staff of the DEIMOS beamline and of Centro di Microscopie Elettroniche "Laura Bonzi", CNR, Sesto Fiorentino for the experimental support. Funding from the European Research Council through the Advanced Grant “MolNanoMas” (267746), from the Italian MIUR through FIRB projects “NanoPlasMag” (RBFR10OAI0), “Nanomagneti molecolari su superfici metalliche e magnetiche per applicazioni nella spintronica molecolare” (RBAP117RWN) and “Rete ItalNanoNet” is acknowledged. The financial support from Ente Cassa di Risparmio di Firenze and Fondazione Cariplo (2010–0612) is also acknowledged.

Received: ((will be filled in by the editorial staff))
Revised: ((will be filled in by the editorial staff))
Published online on ((will be filled in by the editorial staff))

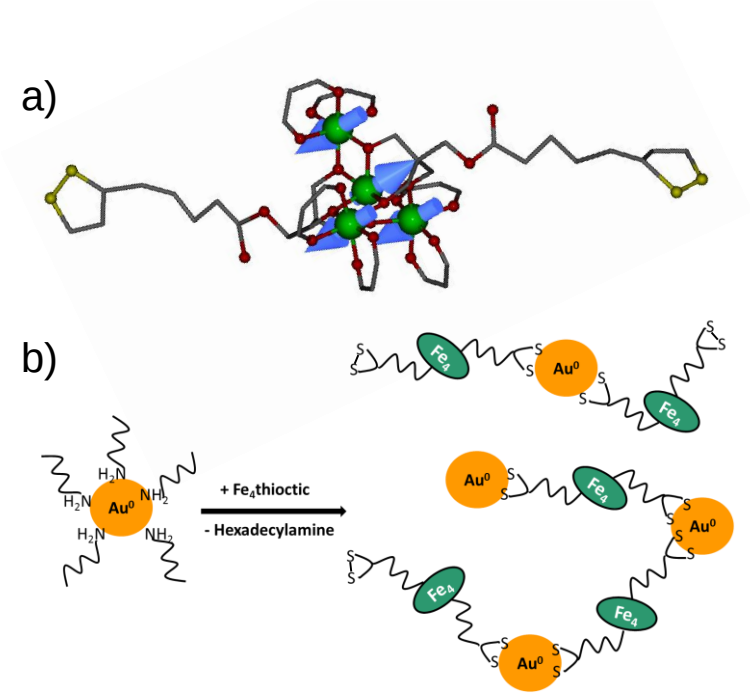

Figure 1. a) Structure of Fe_4thioctic Single Molecule Magnet with the blue arrows indicating the spins' arrangement in the ground state (color code: Fe, green; S, yellow; O, red; C, grey, hydrogen atoms and *tert*-butyl groups of the β-diketonate ligands are omitted for clarity); b) Schematic representation of the used ligand exchange procedure.

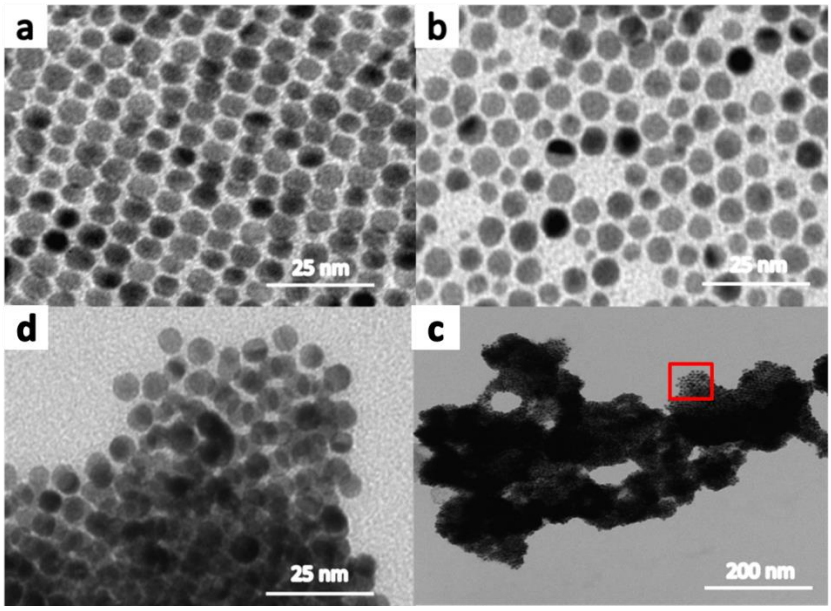

Figure 2. TEM images of HDA-NPs (a), and of the same Au-NPs after functionalization with ADM (b) or with Fe_4thioctic (c). Image d is a magnification of the part of figure c contained in the red rectangle.

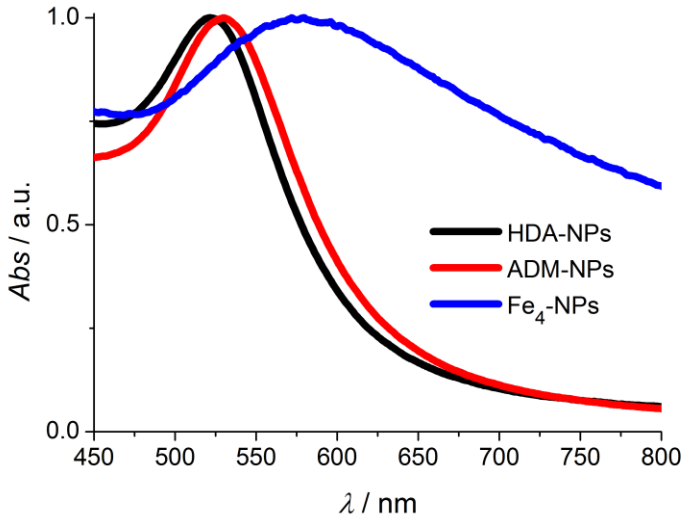

Figure 3. Electronic spectra (normalized at the plasmon resonance peak) of the three types of investigated NPs in CH_2Cl_2 solution.

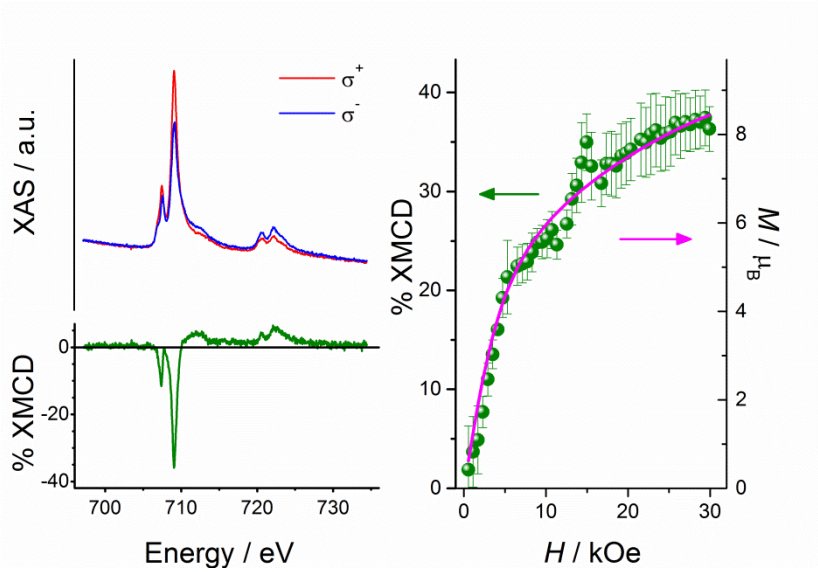

Figure 4. a) XAS and XMCD spectra recorded for Fe_4-NPs at T = 2.2 K and H=30 kOe. b) field dependence of the XMCD signal at 709.1 eV measured at T=2.2 K. The black line corresponds to the magnetization calculated with the anisotropy parameters extracted from EPR spectra.

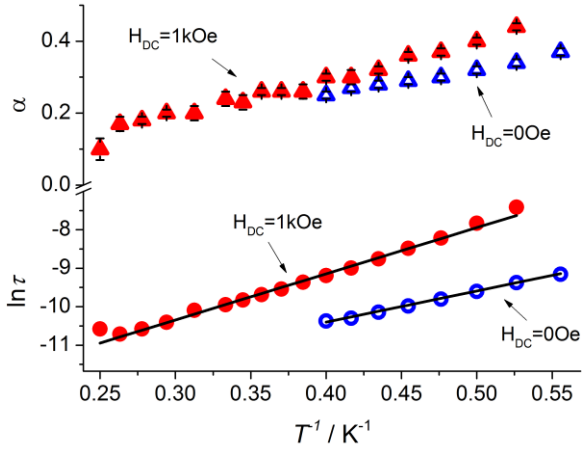

Figure 5. Temperature dependence of the relaxation time (τ) for Fe_4-NPs in static fields H = 1 kOe (red solid circles) and H = 0 Oe (blue open circles); the black lines represent the fits to the Arrhenius law. The upper part of the figure presents the α values extracted from magnetic data at H = 1 kOe (red solid triangles) and at H = 0 Oe (blue open triangles).

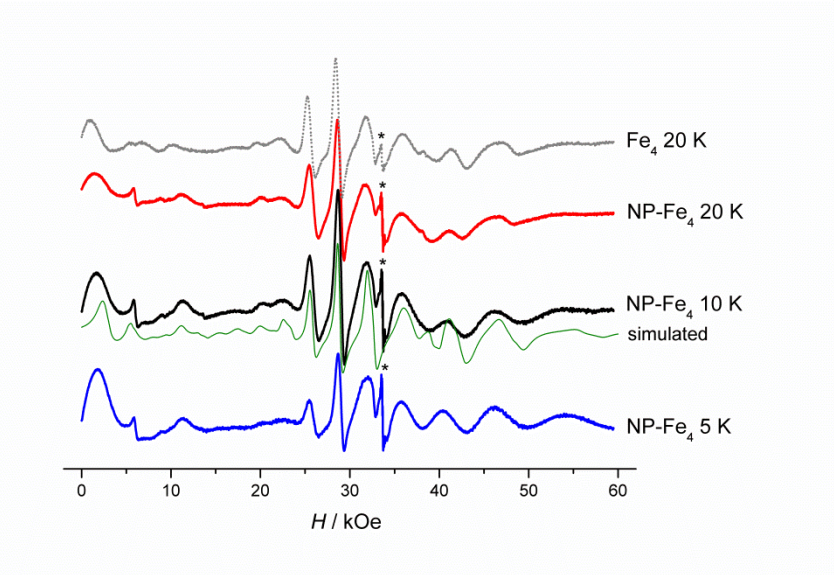

Figure 6.Temperature dependence of W-band EPR spectrum of Fe4-NP (thick blue, black and red lines) and best simulation (thin green line) for the T = 10 K spectrum (parameters reported in the text). The gray line represents the spectrum of microcrystalline Fe_4thioctic at T = 20 K.

TOC Keyword: Hybrid nanomaterials

F. Pineider, L. Poggini, E. Otero, M. Mannini, L. Sorace, C. Sangregorio, A. Cornia, and R. Sessoli*

Title : Grafting Single Molecule Magnets on Gold Nanoparticles

A novel hybrid nanomaterial is obtained by functionalizing gold nanoparticles with a tetrairon(III) Single-Molecule Magnet containing two 1,2-dithiolane end groups, which promote aggregation of the Au nanoparticles. The presence of intact Fe_4 molecules is proven by synchrotron-based XAS and XMCD spectroscopy, while a detailed magnetic characterization confirms the persistence of SMM behavior, thus opening interesting perspectives in the field of molecular spintronics.

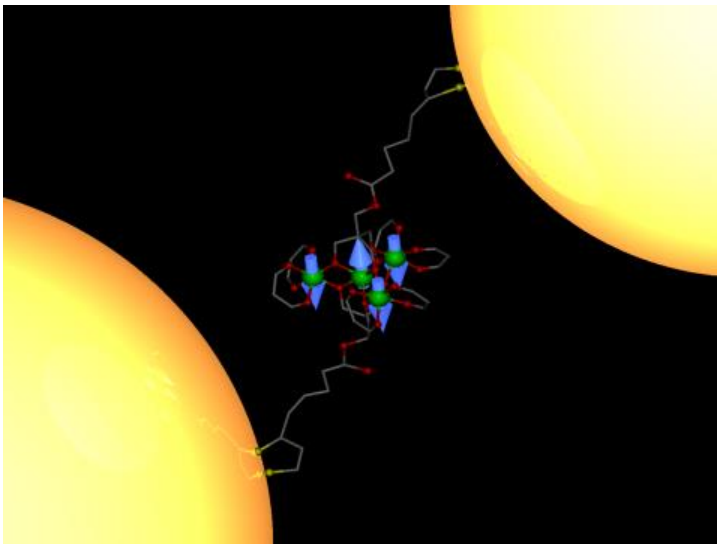

Page Headings
Left page: Mauro Perfetti et al.
Right page: Single Molecule Magnets on Gold Nanoparticles

SUPPORTING INFORMATION

I. Synthetic procedures

Unless otherwise stated all reagents and solvents were purchased from Sigma Aldrich and used as received without further purification.

1. 3-Hydroxy-2,2-bis(hydroxymethyl)propyl 5-(1,2-dithiolan-3-yl)pentanoate

Diethylether was pretreated with $CaCl_2$ overnight, filtered and distilled from its sodium benzophenone ketyl solution under nitrogen. Methanol was carefully dried by treatment with $Mg(OMe)_2$ and distilled prior to use.

Column chromatography was performed using silica gel (Carlo Erba, 0.06-0.200 mm). All the synthesized organic compounds were confirmed by analytical thin-layer chromatography (TLC) on silica gel glass plates (Merck 60 F254). ^{1}H NMR spectra were recorded at 302 K with a Bruker FT-DPX200 NMR spectrometer. Proton chemical shifts are given in ppm downfield from TMS.

2,6,7-Trioxabicyclo[2.2.2]octan-4-yl-methanol (**1**) was synthesized following a literature procedure.[1, 2] Compound $[Fe_4(thioctic)_6(dpm)_6]$ was prepared as described elsewhere,[3] but the tripodal ligand H_3thioctic (**4**) was synthesized using a modified procedure which gives a much improved yield (from 30 to 65%). After the Steglich esterification of (±)-α-lipoic (thioctic) acid with **1**, the bicyclic orthoester **2** was hydrolyzed in 1,4-dioxane/water in very mild acidic conditions (HCOOH). At variance with Ref. 3, the reaction was stopped as soon as conversion to the monoformate **3** was complete and the product purified by column chromatography. Final hydrolysis to **4** was carried out by prolonged heating in a water/1,4-dioxane mixture.

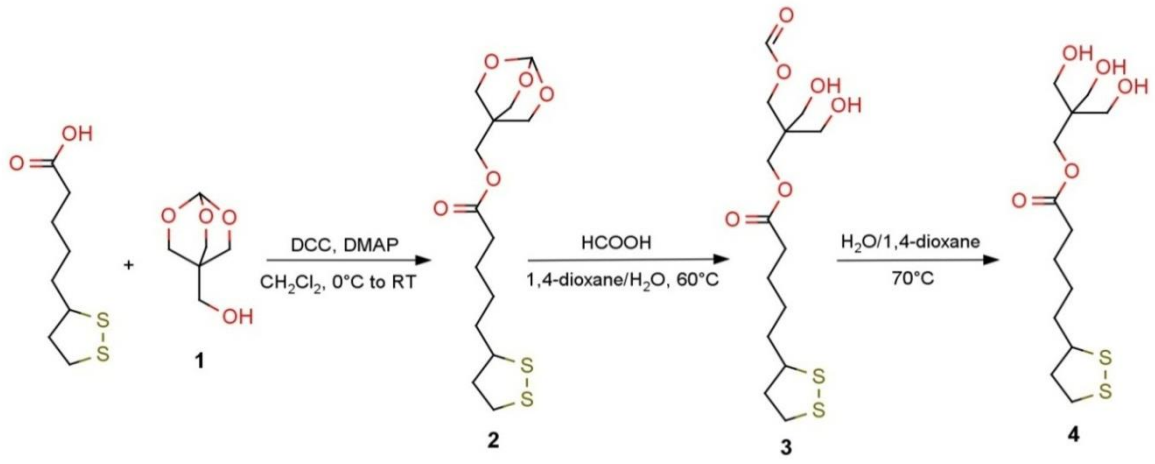

Figure S1: 3-hydroxy-2,2-bis(hydroxymethyl)propyl 5-(1,2-dithiolan-3-yl)pentanoate.

In a three-necked round-bottomed flask fitted with a condenser and a nitrogen inlet, anhydrous degassed dichloromethane (20 mL) was cooled down to 0°C under nitrogen in an ice-water bath. (±)-α-Lipoic acid (0.596 g, 2.89 mmol), compound **1** (0.440 g, 3.01 mmol), *N*,*N*′-dicyclohexylcarbodiimide (DCC, 1.192 g, 5.777 mmol) and 4-dimethylaminopyridine (DMAP, 0.036 g, 2.9 mmol) were added in sequence with stirring. The reaction was continued at 0°C for 4 hours, then at room temperature for 15 hours. The white solid (*N*,*N*′-dicyclohexylurea) was filtered off on a G3 frit and washed with anhydrous dichloromethane (0.580 g). The combined liquid phases were evaporated at reduced pressure to give crude ester **2** as a yellow oil (1.543 g), which was dissolved in 1,4-dioxane:water 2:1 v/v (30 mL). Addition of formic acid (0.2 mL) under stirring caused immediate precipitation of additional white solid. The mixture was stirred for 40 min. at room temperature, then was warmed up to 60°C and kept at this temperature for 20 hours. TLC on the reaction mixture (dichloromethane:methanol 9:1 v/v) showed progressive consumption of **2** (R_f = 0.82) to give the monoformate **3** (R_f = 0.49) and a minor amount of **4** (R_f = 0.36). The mixture was cooled down in an ice-water bath and *N*,*N*′-dicyclohexylurea was filtered off and washed with 1,4-

dioxane (10 mL) on a G3 frit (0.570 g). Solvent removal from the combined liquid phases under vacuum at room temperature yielded the crude monoformate **3** as a dense yellow oil (1.09 g). The latter was passed through a short silica gel column (3×12 cm, from pure dichloromethane to dichlormethane:methanol 9:1 v/v). Fractions containing compounds **3** and **4**, which formed clearly visible yellow bands, were combined to give a yellow oil after solvent evaporation (1.02 g). The oil was dissolved in 1,4-dioxane (25 mL) and water (100 mL) was added with vigorous stirring. The resulting emulsion gradually turned into a single phase upon continuous stirring at 70°C. After 44 hours, TLC confirmed virtually complete conversion of **3** to **4** and the reaction was stopped. After removal of the solvent under vacuum at room temperature, the product was chromatographed on a short silica gel column (5×17 cm) (dichloromethane:methanol from 20:1 to 14:1 v/v) to afford **4** as a yellow oil that solidified upon prolonged standing at -10 °C (0.607 g, 65% overall yield). The ^{1}H-NMR spectroscopic properties of the product in CD_3OD were identical to those already presented in Ref. 3. In that paper, the highest-field signals have been misreported; the correct spectral data are δ = 1.77–1.40 (m, 6H, –C*H*$_2$C*H*$_2$C*H*$_2$–).

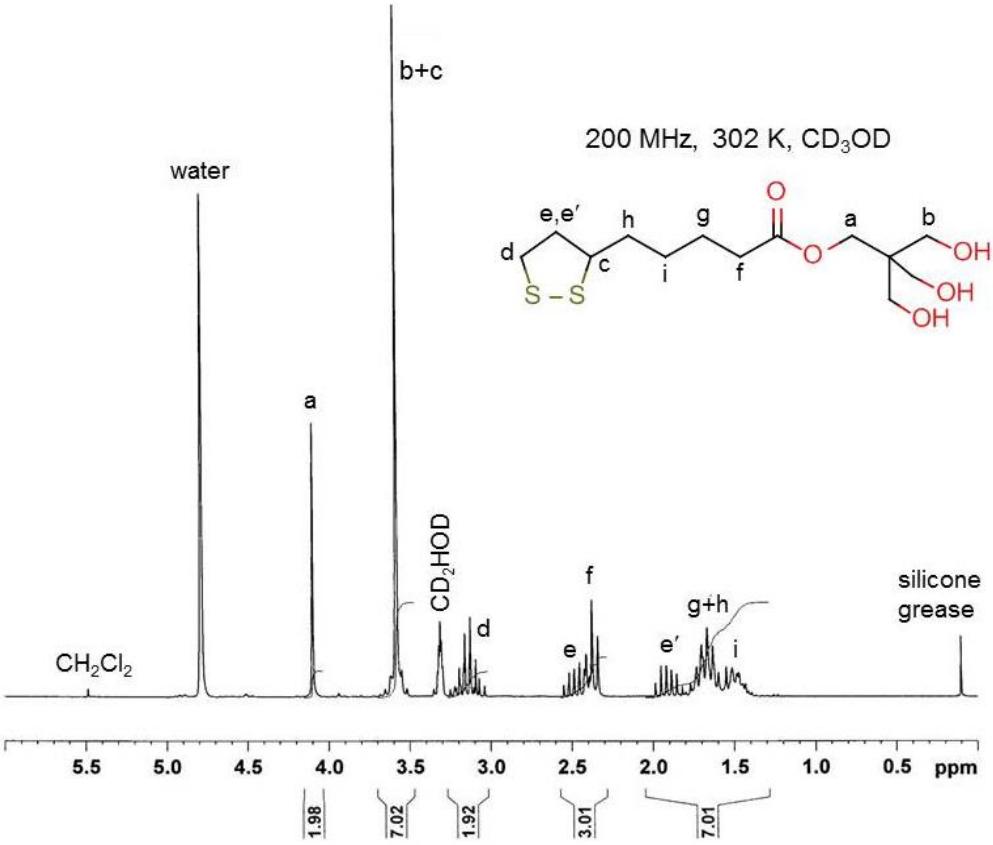

Figure S2: NMR spectrum of 3-hydroxy-2,2-bis(hydroxymethyl)propyl 5-(1,2-dithiolan-3-yl)pentanoate.

Fe_4thioctic was synthetized as described elsewhere.[3]

2. Methyladamantyl 5-[1,2-dithiolan-3-yl]pentanoate (ADM)

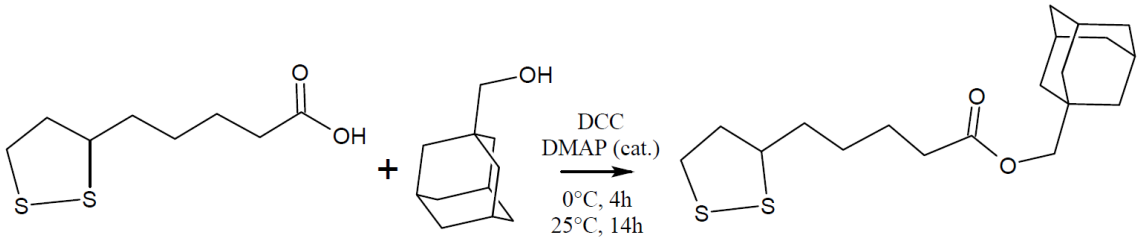

Figure S3: Schematic view of the reaction between thioctic acid and 1-adamantanemethanol to give methyladamantyl 5-[1,2-dithiolan-3-yl]pentanoate (ADM).

Among the several esterification techniques reported in the literature only few methods deal with adamantane derivatives.[4] The synthetic procedure we chose is similar to one previously described for the esterification of (±)-α-lipoic acid.[5] Initially 1-adamantanemethanol (4.0 g, 24 mmol) and (±)-α-lipoic acid (4.77 g, 23 mmol) were solubilized in dry degassed CH_2Cl_2 (100 ml) to obtain a yellow solution. Under N_2 flow, the solution was cooled to 0°C before the addition of DMAP (282 mg, 2.3 mmol) and DCC (4.75 g, 23 mmol). After 4 h of vigorous stirring, the reaction was slowly warmed up to room temperature and stirred for additional 14 h to give a white suspension. Solid *N,N'*-dicyclohexylurea was removed by filtration *in vacuo*, and the solution was subjected to column chromatography [SiO_2: CH_2Cl_2/Hexane=9:1]. The fractions containing the product were combined and the solvent removed *in vacuo* to give a yellow oil (7.81 g, yield 96%).

^{1}HNMR (CD_2Cl_2, 400MHz, 25°C, Me_4Si): δ (ppm)=1.40-1.52 (m, 2H), 1.54-1.55 (d, 6H), 1.62-1.76 (m, 6H+4H), 1.87-1.95 (m, 1H), 1.98 (m, 3H), 2.31-2.35 (t, 2H), 2.42-2.50 (m, 1H), 3.09-3.22 (m, 2H), 3.55-3.62 (m, 1H), 3.66 (s, 2H).

Elemental analysis for $C_{19}H_{30}O_2S_2$: Experimental C,64.4%, H,8.5%, N,0%. Theoretical C,64.4%, H,8.5%, N,0%.

II. Damage proof

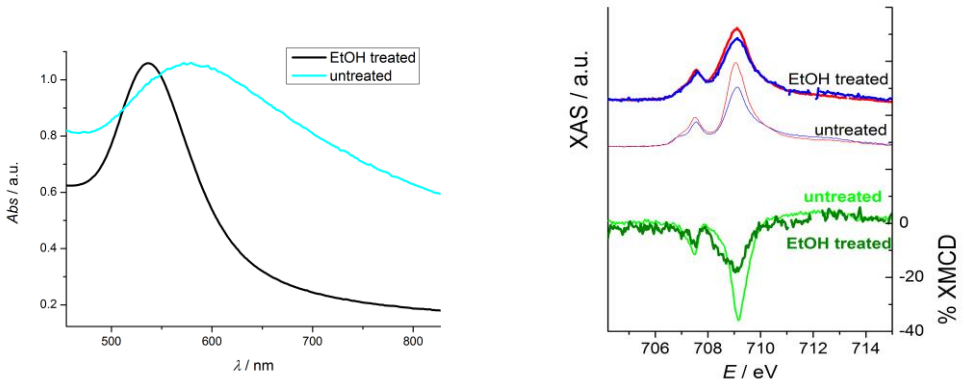

Figure S4. Left: UVVis spectra of the pristine and EtOH treated Fe_4-NPs in dichloromethane solution. Right: XAS/XMCD spectra of the pristine and EtOH treated Fe_4-NPs measured at T = 2.2 K and H =30 kOe.

Here we report evidences that the disruption of aggregates of Fe_4NPs is achieved upon damaging the Fe_4 core by adding EtOH.

EtOH (15 ml) was added to a solution of 5 mg of Fe_4NPs in 5 ml of CH_2Cl_2, then the mixture was centrifuged and the precipitate was redispersed in CH_2Cl_2.

The UV-Vis spectrum of Fe_4NPs after treatment with EtOH shows the recurrence of the plasmonic peak typical of pristine gold NPs while XAS/XMCD at Fe L_3 edge evidences a broadening of the absorption and a significant (more than 50%) reduction of the magnetic signal, confirming the damaging of the SMMs decorating the NPs.

III. Statistics

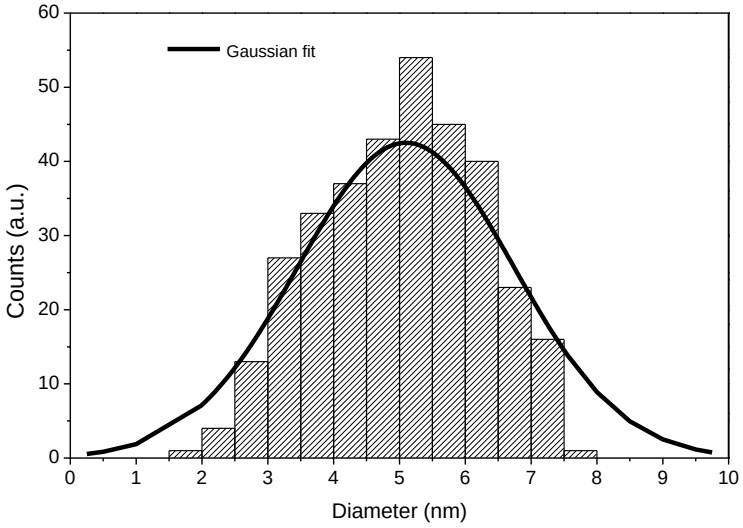

Figure S5: Size distribution of the synthesized HDA-NPs obtained from TEM images, fitted with a Gaussian function (black line). The NPs diameter was measured with ImageJ for 300 NPs.

IV. Geometrical calculations on the steric hindrance of ADM and Fe_4thioctic and on the maximum coverage of gold NPs

For the ligand exchange process we used an excess of ligand (ADM or Fe_4thioctic), with respect to the amount required for complete NPs coverage.

For an estimation of the amount of Fe_4thioctic or ADM on the NPs surface, we developed a simple method based on geometrical assumptions. We calculated the total surface area of NPs assuming an effective diameter with $d_{eff} = d_{NP} + 2\lambda$ where d_{NP} is the diameter obtained by the TEM statistic and λ is the total length of the organic chain from the 1,2-dithiolane ring to the

oxygen of the ester bond. After that, we divided that surface area by a ligand hindrance estimated as $A_{hindr} = \pi(d_{molecule}/2)^2$, where $d_{molecule}$ is an approximate diameter obtained by the crystallographic structure of the molecules(neglecting the area necessarily uncovered by the circles). For ADM we used the structural information extracted from 1-adamantanemethanol d_{ADM} was assumed to correspond to the distance between the two opposite hydrogen atoms in the cyclohexane ring of adamantane (d_{ADM} = 0.472 nm), while in the case of Fe_4thioctic we considered the distance between the hydrogen atoms of two opposite dipivaloylmethanide groups in the molecule, obtaining d_{Fe4} = 1.844 nm. Finally we calculated the weight percentage of Fe_4 and ADM in our samples taking into account the different weight of NPs with different size. The final result produced from the dedicated algorithm was 12.0% for Fe_4thioctic and 27.3% for ADM. These values are an overestimation because of several approximations such as the absence of thermal motion, disorder, and bending of the chains. Moreover, the number of SMM molecules per NP, reported in Figure S6, is evaluated assuming that each Fe_4 links one NP, which is an unrealistic upper limit case, considering that a network of NPs is formed.

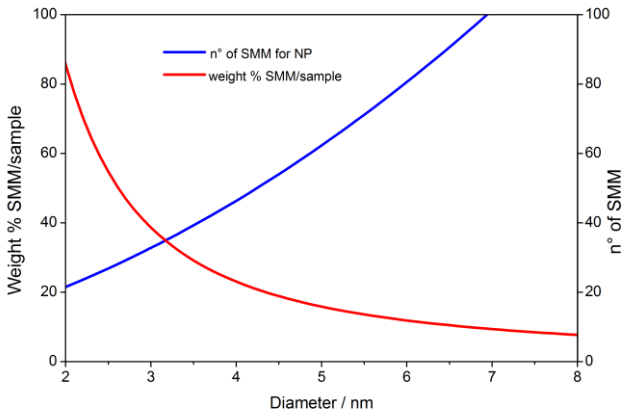

Figure S6: The right scale refers to the theoretical maximum coverage of NPs by Fe_4 molecules as a function of the NPs diameter, in terms of number of Fe_4 molecules per NP (blue) and of weight percentage of Fe_4 molecules (red).

V. UV-Vis spectra

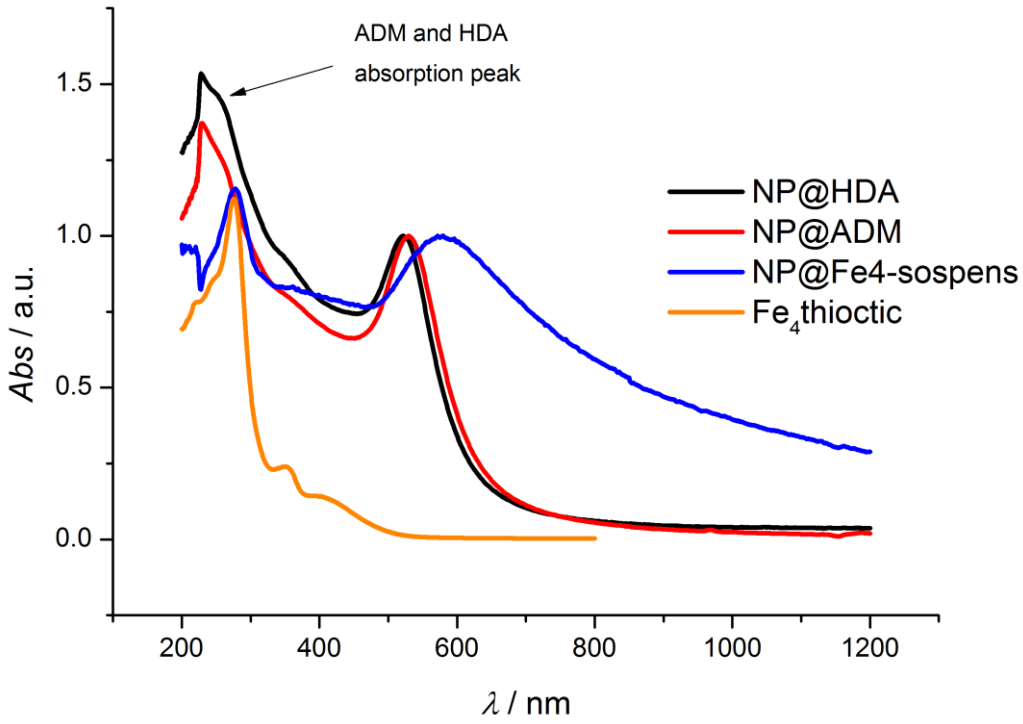

Figure S7: UV-Vis spectra of HDA- (black line), ADM- (red line) and Fe_4- (blue line) NPs normalized ad the plasmon resonance peak. The orange line refers to a solution of pristine Fe_4thioctic in CH_2Cl_2.

VI. NMR Spectra

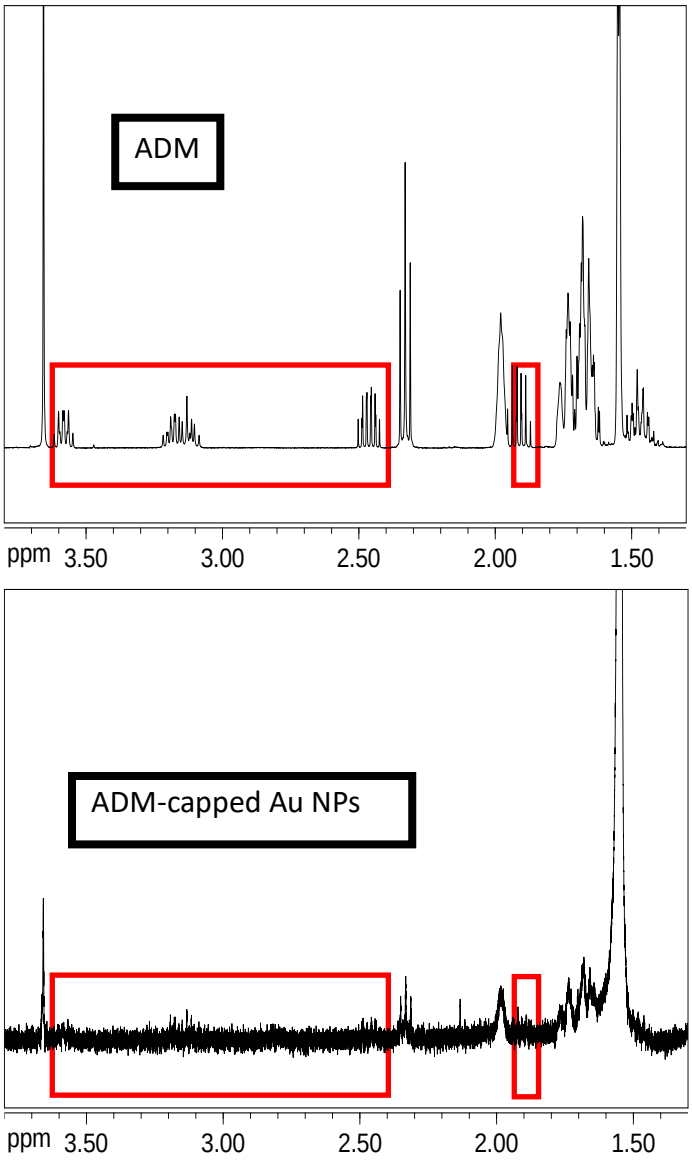

Figure S8: 400-MHz ^{1}H NMR spectra of ADM and ADM-NPs in CD_2Cl_2. The red rectangles highlight the signals from 1,2-dithiolane ring protons.

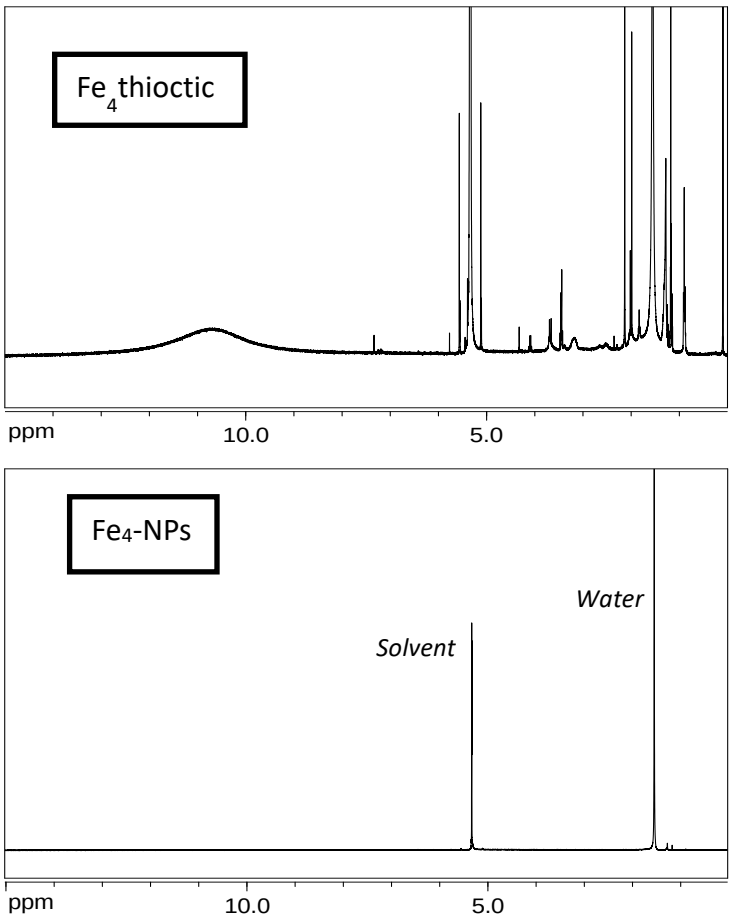

Figure S9: 400-MHz ^{1}H NMR spectra of Fe$_4$thioctic and Fe$_4$-NPs in CD_2Cl_2.

VII. XPS spectra

XPS experiments were carried out in a ultra-high vacuum (UHV) apparatus consisting of one chamber with a base pressure in the low 10^{-9} mbar range. Non-monochromatised Al *Kα* radiation was used. The angle between the analyser axis and the X-ray source was 54.44° and the semicone angle of acceptance of the analyser was 4°. The XPS spectra were measured with a fixed pass energy of 44 eV. The binding energy (BE) scale was calibrated setting the C1s photopeak of graphite to 284.4 eV.[6]

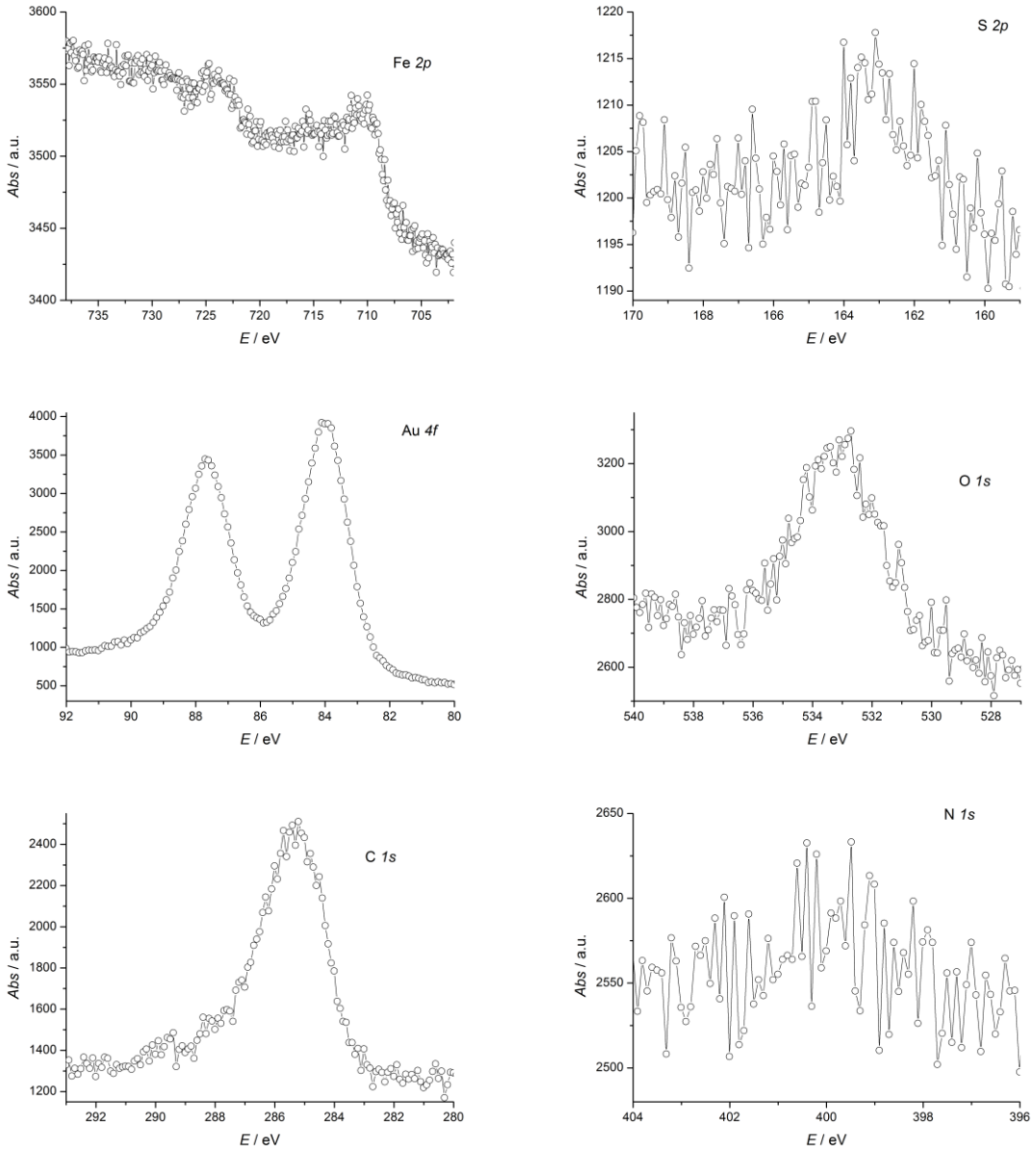

Figure S10: XPS spectra in the Fe2p, S2p, Au4f, O1s, C1s and N1s regions for Fe_4-NPs obtained by drop-casting a CH_2Cl_2 dispersion on HOPG.

VIII. Magnetic measurements for HDA NPs and ADM NPs

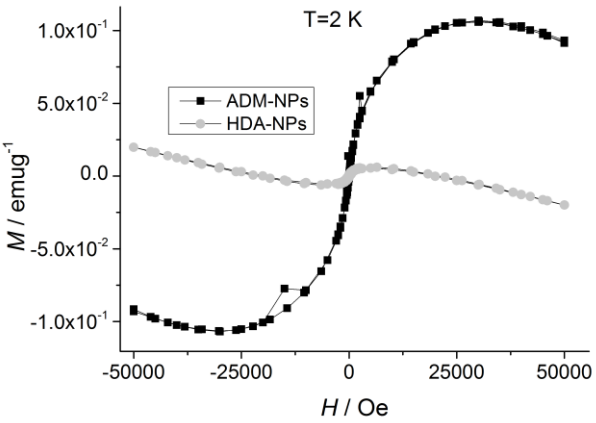

Figure S11: Hysteresis curve for HDA-NPs (gray dots) and ADM-NPs (black squares) recorded at T=2 K.

IX. Magnetic measuremets for Fe_4-NPs

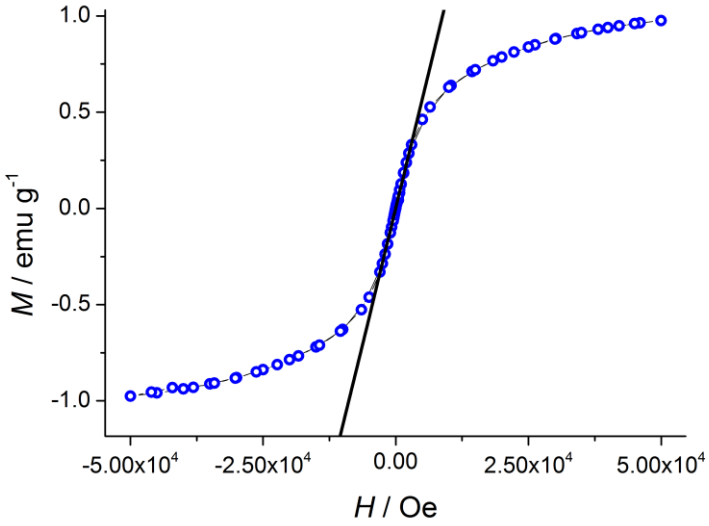

Figure S12: Hysteresis curves performed at T = 2.0 K, along with the linear fitting used to obtain the initial magnetic susceptibility (black line).

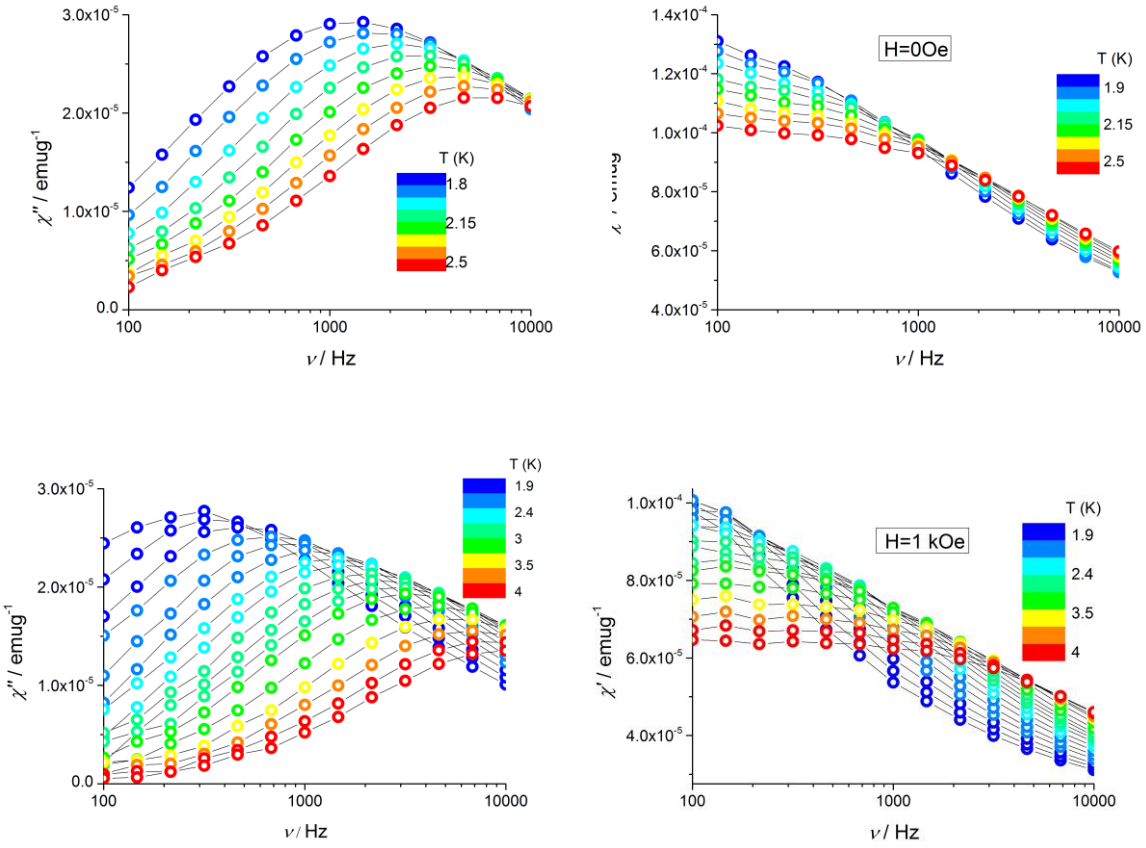

Figure S13: Imaginary (left column) and real (right column) components of the ac magnetic susceptibility in a frequency range between 100 and 10000 Hz for Fe_4-NPs. Data in the upper row have been recorded in zero applied field and in the temperature range from 1.8 to 2.5 K. Data in the lower row have been recorded at H =1 kOe and in the temperature range from 1.9 to 4.0 K.

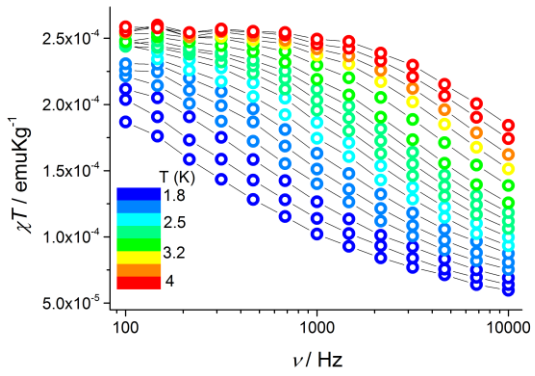

Figure S14: Molar χT product versus frequency in a range of T from 1.9 to 4.0 K.

X. Bibliography

[1] a) X. Hou, X. Zhang, Y. Fang, S. Chen, N. Li, Q. Zhou, J. *Nanopart. Res*. **2011**, 13, 1929-1936; b) S. Peng, Y. Lee, C. Wang, H. Yin, S. Dai, S. Sun, *Nano Res.* **2008**, 1, 229-234.
[2] a) A. B. Padias, H. Hall Jr, D. A. Tomalia, J. McConnell, *J. Org. Chem*. **1987**, 52, 5305-5312; b) A. B. Padias, H. Hall Jr, *Macromolecules* **1982**, 15, 217-223.
[3] M. J. Rodriguez-Douton, R. Sessoli, A. Cornia, *Polyhedron* **2011**, 30, 2960-2964.
[4] S. M. Iossifidou, C. C. Froussios, *ChemInform* **1997**, 28, 1355.
[5] R. Klajn, L. Fang, A. Coskun, M. A. Olson, P. J. Wesson, J. F. Stoddart, B. A. Grzybowski, *J. Am. Chem. Soc*. **2009**, 131, 4233-4235.
[6] P. Kowalczyk, O. Mahapatra, D. McCarthy, W. Kozlowski, Z. Klusek, S. Brown, *Surf. Sci*. **2011**, 605, 659-667.